J. Condensed Matter Nucl. Sci. 29 (2019) 52–74

Research Article

Steps to Identify Main Parameters for AHE Generation in Sub-micrometric Materials: Measurements by Isoperibolic and Air-flow Calorimetry

Francesco Celani,* B. Ortenzi and A. Spallone
INFN-LNF, Via E. Fermi 40, 00044 Frascati (RM), Italy

C. Lorenzetti, E. Purchi, S. Fiorilla, S. Cupellini, M. Nakamura, P. Boccanera and L. Notargiacomo
International Society for Condensed Matter Nuclear Science (ISCMNS-L1), via Cavour 26, 03013 Ferentino (FR), Italy

G. Vassallo
Department of Industrial and Digital Innovation, University of Palermo, Viale delle Scienze, 90128 Palermo (PA), Italy

R. Burri
IETC Laboratories (www.ietclab.org), 6827 Brusino Arsizio-CH, Italy

Abstract

In 2011, we introduced the use of constantan alloy in LENR, in the form of long and thin wires as a hydrogen dissociation promoter. We disclosed for the first time the reason for the choice of such material at IWAHLM-12 Workshop (2017), hypothesizing it was the initiator of the reaction in Andrea Rossi's experiment. We developed a specific treatment to increase the dimensionality of wire surface through the application of high peak power pulses. The wire is inserted in fiberglass . . . (continued in the next page)
 ISSN 2227-3123

Keywords: Anomalous Heat Excess (AHE), Electro-migration phenomena, H_2 and/or D_2 absorption at high temperatures into constantan, $H_2 \rightarrow 2H$ dissociation by constantan, Isoperibolic and air-flow calorimetry, Low work function materials, Noble gases, Spontaneous voltage generation along hydrogen-absorbing wires, Surface-modified Cu–Ni–Mn alloy, Thermionic effect

*Corresponding author. E-mail: franzcelani@libero.it.

 ISSN 2227-3123

(continued from the title page)

sheaths, made up of micrometric fibers, impregnated with a solution of an electron-emitter element (Sr). Later, we added Fe and K to the wire surface and the sheaths and adopted the procedure of making equally spaced knots along the wire to produce thermal and magnetic gradients. We also pointed out that the addition of noble gases with low thermal conductivity, and in particular xenon, to the H_2/D_2 atmosphere, produces a considerable rise of temperature in the reactor, maybe because those gases acting as catalyzers in the generation of excess power. Measurements were always performed with isoperibolic calorimetry, which has the advantage of producing non-equilibrium conditions that favor the generation of anomalous heat excess (AHE). With this procedure, we reached a gain of almost a factor 2 at the highest temperature, although with limited stability over time. In this paper, we present SEM observations and EDX analyses of the wire before and after applying the treatment. We have also conducted a series of experiments using air-flow calorimetry. The calorimeter consists of an insulating Styrofoam box whose internal walls are covered with a thick foil of aluminum; the external wall of the reactor was covered with a double layer of black and thick aluminum foil to homogenize temperature. The calorimeter contains the reactor and a halogen tungsten lamp inside a dummy reactor used for calibrations. Even with the air-flow calorimetry approach, which does not produce the most appropriate conditions for AHE, we have obtained excess power, although in quite lower amounts. The best results are: (a) with 100-μm diameter wire, D_2 at 1 bar, input power 90 W, the AHE was over 12 $\pm$2 W, but after 1 day the wire broke and (b) with 200-μm diameter wire, Xe–D_2 mixture each at 0.1 bar and input power of 120 W, AHE was 6–7 W stably for weeks.

1. Introduction: The Choice of Constantan

In 2011, we initiated a research program aimed to increase the magnitude and reproducibility of the so-called *Anomalous Heat Effects* (AHE) as the main result of the occurrence of *Low Energy Nuclear Reactions* (LENR), preferably using *low-cost materials*.

For this purpose, we focused the program from the very beginning on the study of constantan, an alloy of nickel and copper ($Cu_{55}Ni_{44}Mn_1$, abbreviated as CNM or Cst) developed by E. Weston in 1897, instead of other metals that have been extensively studied over the years, such as:

- Palladium (F. Paneth as Pd compounds, and in particular in the form of asbestos in 1926 [1], M. Fleischmann and S. Pons using electrolytic loading in 1989 [2]).
- Ti (S. Jones [3] F. Scaramuzzi since 1989 [4]).
- Ni (S. Focardi and F. Piantelli as bulk-shaped rods since 1991 [5], A. Rossi and B. Ahern as powders in 2008).

At that time, CNM alloy was quite unusual in the field of LENR research and we selected it as a possible substitute for the previously used metals because of the disclosure of Rossi's invention during the demonstration held in Bologna in January 2011 (which was not considered conclusive by the LENR community). We supposed the presence of a *hidden factor* behind the successful AHE generation in early Rossi's experiments that, likely, was not immediately recognized. To our best knowledge, such early experiments took place in 2007 while A. Rossi was collaborating with B. Ahern in the United States.

We would like to emphasize that the real reason for the choice of constantan in our research program was presented for the first time in public and discussed in detail at IWAHLM-12 (5–9 June 2017, Asti-Italy, an International Workshop organized since 1996 by B. Collis). Later on, several scientific meetings on LENR field were devoted to analyzing and discussing such arguments. Among others, the most important were held at the Aeronautic section of the Italian Army (end of June 2017, Rome), and at the 70th Anniversary of ANDI (Associazione Italiana Degli Inventori – Italian Association of Inventors, November 2017, Rome).

After deeply considering Rossi's experimental set-up, we came up with the hypothesis that the *real and main catalyst or initiator* of the reaction with gaseous hydrogen was not the nickel itself, but the *thermocouple* inserted in the reactor with Ni nano-powders. In particular, we refer to J-type (Fe–Constantan) thermocouple, suitable for the temperature range of most experiments (<750°C). This type of thermocouple is especially convenient because of its low cost and high sensitivity (about 50 μV/°C). Furthermore, we believed, based on our experience, that *this thermocouple could be partially damaged after several tests, leading to the activation of its surface* and that the insulating and protective material covering the thermocouple – a kind of glass – may contribute as well to the observed phenomena.

Later, in June 2011, we found a paper of S. Romanowski and collaborators [6] supporting our empirical considerations. On the basis of computer simulations, they show that Ni–Cu alloy, such as constantan, may provide an extremely large amount of energy (up to 2–3 eV for a wide range of Ni–Cu ratio) for the catalytic dissociation of hydrogen molecules to the atomic state ($H_2 \rightarrow 2H$) (Table 1).

Similar catalytic properties can also be expected with deuterium gas and they actually have been retroactively noticed in electrolytic and gaseous experiments carried out by our group since 1989. At that time results obtained in comparative tests of Pd and Ni in electrolytic environmental conditions did not have a clear explanation. After repeated cycles of cathodic/anodic regimes and high/low current densities, we observed that Cu (and Ag) could occasionally show-up in our electrolytic cell, because of contamination coming from the electrical connections (wires of Cu-Ag covered by PTFE) due to the corrosion mediated by LiOD–D_2O vapors and be deposited on Pd surfaces and even more on Ni. The measured excess heat was, some times, larger in the case of the less "noble" Ni than with Pd.

Another fact that made us more confident about the adoption of such material was the discovery of a patent filed in 1993 [7] – brought to our attention by our coworker G. Vassallo in summer 2012 – where B. Ahern appears as the first inventor. In this patent, Cu–Ni is reported as a good candidate for obtaining AHE, especially when at *nanometric dimensions* or under the form of *alternating layers* of copper and nickel. Such indication encouraged us to use and further develop our technique for the preparation of a multilayered and nanostructured texture by means of electrical short-duration pulses of very high peak power.

Table 1. Predicted value of dissociation energy for H_2 dissociation reaction with different materials [6]. The best catalytic material is $Ni_{0.375}Cu_{0.625}$ with more than 3 eV, the worst is Ag.

Material composition	DE (eV) for hydrogen dissociation ($H_2 \rightarrow 2H$)
$Ni_{0.375}\,Cu_{0.625}$	3.164
$Ni_{0.625}\,Cu_{0.375}$	2.861
$Ni_{0.8125}\,Cu_{0.1875}$	2.096
Ni	1.736
$Ni_{0.1825}\,Cu_{0.8175}$	1.568
$Ag_{0.8125}Pd_{0.1875}$	0.572
$Ag_{0.625}Pd_{0.375}$	0.560
$Ag_{0.325}Pd_{0.675}$	0.509
$Ag_{0.1875}Pd_{0.8125}$	0.509
Pd	0.424
Cu	–1.110
Ag	–1.416

2. Wire Treatment

In order to increase the surface area of CNM wires, we apply to them several hundred electric pulses, typically with a duration of 50 ms (recently up to 70 ms), with a rather large peak power (15–20 kVA/g). In this way, we reach a surface temperature of 700–1000°C in air, that point at which constantan starts to oxidize showing the formation of a spongy sub-micrometric texture. We believe that such behavior is due to the rapid rise in temperature followed by rapid cooling (quenching), which leads to some phase separation with the formation of separated islands of nickel-rich or copper-rich phases, a supposition *confirmed by EDX analysis*.

It is likely that a skin effect (pulse rise-time 1 μs) *concentrates* most of the current, and therefore the power, at the surface of the wire, with predictable effects on the increase of temperature and its gradient.

When we first looked at the treated materials with SEM–EDX after pulsed oxidation, we were surprised to note that the wire surface displayed the presence of mixed oxides of copper and nickel (Cu_xO_y, Ni_wO_z) arranged in a multilayer and sub-micrometric structure.

We would like to highlight that the material prepared per this procedure shows a reduced tendency to self-sintering. Consequently, the inert material that is often added to reduce sintering problems (e.g. ZrO_2 chosen by Yoshiaki Arata since 2002 for nano-Pd) is now replaced with structures that can possibly absorb some amounts of hydrogen and take part in the exothermic reactions. Finally, the pristine CNM is the substrate where the sub-micrometric materials of various composition are supported.

For the sake of clarity, we point out that we do not have precise control of nanoparticle dimensionality as in Arata's procedure with the use of melt-spinning and quenching processes, by which he obtains 2–15 nm nanoparticles with Pd_35% over ZrO_2_65%.

We occasionally observed that the oxidized and partially reduced structures on constantan wires may detach and fall off, affecting negatively the outcome of the experiment. Such adverse effects increase after H/D absorption and several thermal cycles (e.g. 20→400 – 700→20°C).

In our experimental set-up, constantan has been used in the form of long ($l = 1$ m) and thin wires ($\Phi = 200\,\mu$m; weight per unit length 0.28 g/m), whose surface is very smooth before applying our procedure.

3. Importance of Non-equilibrium Conditions

In almost all of our experiments, we realized that having non-equilibrium conditions is a key factor to induce, and possibly increase, any anomaly in the H/Metal systems. Over many years, we noticed that all kinds of *local non-equilibrium conditions* (thermal, electric, H/D concentration, radiation, etc.) play a role in triggering excess power release. Based on this conclusion, in 2015 we introduced a new type of wire geometry, aiming to increase the local thermal gradients.

We already took advantage of fiberglass sheaths, which represent a step-discontinuity to heat transfer from the wire to the local gaseous environment. Such effect further increases if the wire has a current flowing in it, as usual in our experiment; the result is also a large voltage drop along the wire, originating Non-Faradaic Electrochemical Modification of Catalytic Activity (NEMCA) Effect [8] (later independently rediscovered by G. Preparata and E. Del Giudice) and increasing the catalytic activity of constantan wire. After various attempts, we realized that the simplest approach to strengthen the thermal gradients was to introduce several knots in the CNM thin wire.

The steps for the reactor assembly are detailed in Fig. 1. The most critical part is the tightening of the knots, during which the fragile wire can be subjected to damage because of the mechanical stress. Once current I is applied, the knot becomes a current loop that gives rise to a magnetic field whose lines go through the hole and whose strength along the z-axis – directed along the centerline of the loop – is given by:

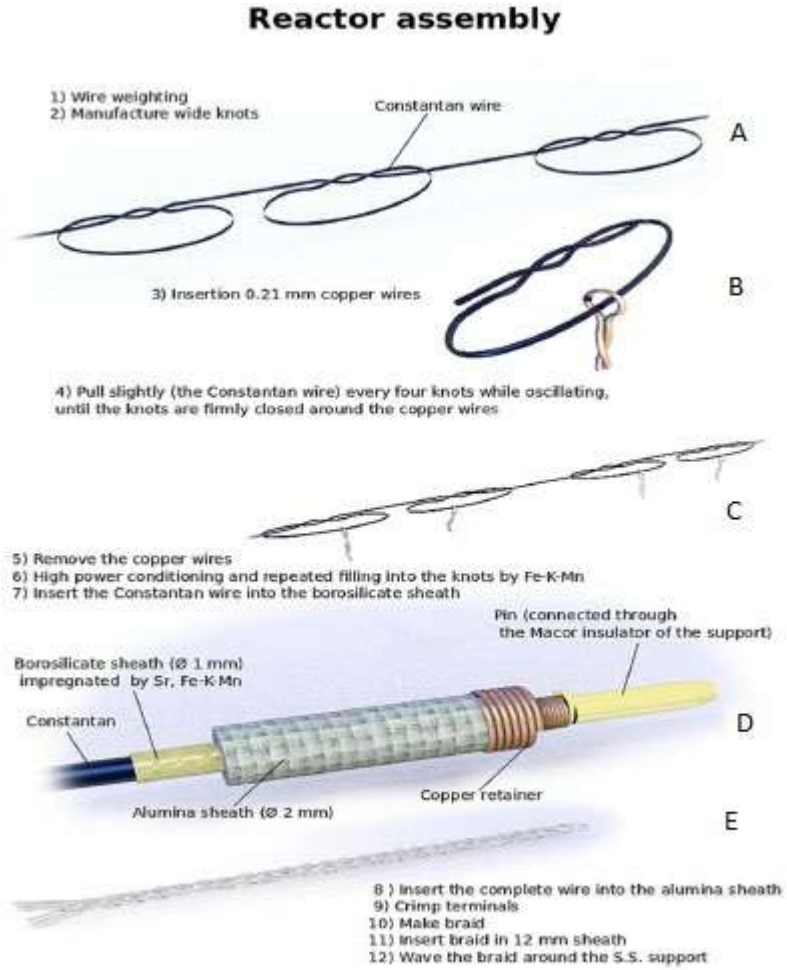

Figure 1. Reactor assembly: (A) Preparation of the knots in the constantan wire. (B) Insertion of the copper wires in order not to completely tighten the knot. (C) Critical point of tightening the node due to possible stress of the constantan wire. (D) After conditioning, insertion of the wires inside the several glass sheaths. (E) Braid of the three wires to be waved around the SS support.

$$B_z = \frac{\mu_0}{4\pi} \frac{2\pi R^2 I}{(z^2 + R^2)^{3/2}}\,, \tag{1}$$

where R is the radius of the loop and z the distance along the z-axis from the loop. Finally, Fig. 2 presents an overview of the reactor once assembled. Note that the core is at the end inserted in a thick-wall borosilicate glass tube. Temperatures are measured at the external wall of the glass tube ($T_{\rm c}$) and at the SS central support ($T_{\rm ss}$) along which the wires are braided inside the reactor.

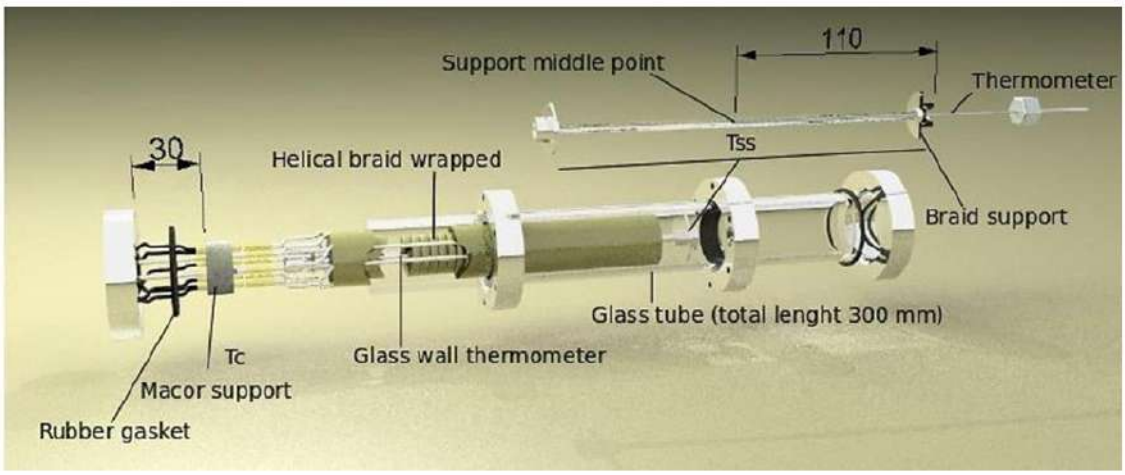

Figure 2. Schematic of the reactor once assembled.

The procedure worked very well and the first results were presented at ICCF20 (Sendai-J**,** October 2016). We compared two 200-μm constantan wires having 41 and 71 knots in terms of their capability of generating AHE and noticed that the excess power is positively correlated with the number of knots. At the beginning, the knots had an

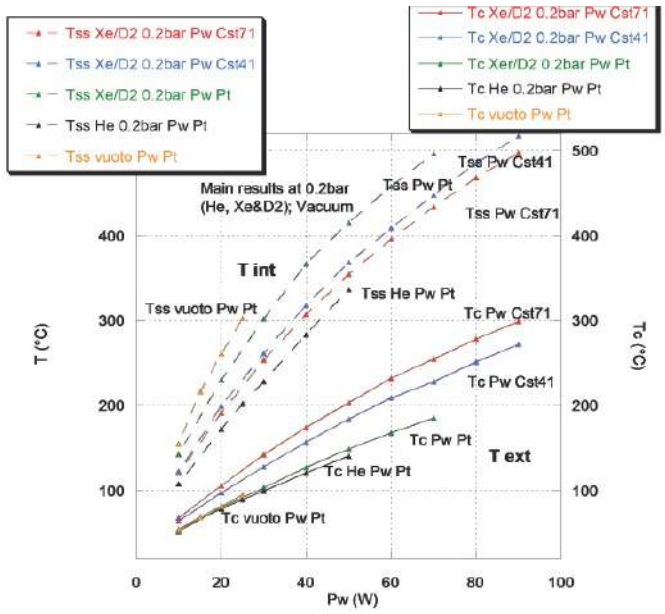

Figure 3. Temperature versus Input Power applied to the reactor in vacuum (P_{w} at Pt), He (P_{w} at Pt), Xe+D_2 mixture (P_{w} at Pt, Cst41, Cst71) atmosphere. A large increase of external temperature T_{c} is observed with respect to Pt case for P_{w} applied to Cst41 and Cst71.

internal diameter in the range of 0.2–0.6 mm; later, it was decreased to 0.15–0.20 mm.

In our experiment, we also had mild excitation thanks to gamma ray arising from commercial Thoriated Tungsten rods (used for TIG welding) positioned outside the glass reactor and inside an airtight small SS tube.

A summary of the results achieved with the above-described set-up is shown in Fig. 3. After calibration in vacuum and in helium atmosphere, the experiments were carried out with a D_2–Xe (50% ratio) gas mixture at 0.2 bar. The choice of xenon is motivated by its low thermal conductivity, in order to increase as much as possible the temperature in the reactor at constant input power. We display the behavior of temperature $T_{\rm ss}$ and $T_{\rm c}$ as a function of input power, for power applied respectively to Pt, 41-knots Cst and 71-knots Cst wire. One can observe the beneficial effect of non-equilibrium conditions, growing $T_{\rm c}$ with the number of knots in the wire.

4. High Peak Power Pulses

Figure 4 shows a sequence of pictures taken with a time frame of about 20 ms when high peak power (HPP) pulses were applied to a constantan wire of 200 μm diameter with knots whose hole has a diameter smaller than 200 μm and at a distance of $\sim$2 cm from each other.

We can observe that the area of the knots is brighter in comparison to the normal part of the wire, meaning that in those sites, higher temperatures are reached, and local thermal non-equilibrium achieved. Such conditions take place also in DC operation. The HPP pulser is based on the well-known capacitive discharge method. Among its performance characteristics are the quite large value of (multiple) capacitor bank used (6600 μF, parallel of ceramics, polyesters, pulse-operated electrolytic), the relatively large repetition rate (0.1 Hz), the fast rise ($<$1 μs) and fall time. The electronic switch is based on four Power MOS arranged in parallel, with up to 100 A of current capability and 450 V of voltage limit. The HPP pulser has to provide the wire enough energy to account for:

(A) The thermal inertia of the wire, which opposes to temperature changes. The heat to be transferred to the wire is given by

$$Q = mc_{\rm p}\Delta T,$$

where *m* is the mass (g), $c_{\rm p}$ is the specific heat (J g^{-1}°C^{-1}), ΔT is the temperature variation (°C).

(B) The power lost by irradiation, given by Stefan–Boltzmann law

$$P = \sigma T^4 S,$$

where $\sigma = 5.67\times 10^{-8}$ W m^{-2} K^{-4}, S the surface of the wire.

(C) The power transferred by convection to the air, given by

$$P = hS\Delta T,$$

where the heat transfer coefficient $h \approx$10 W m^{-2} K^{-1}.

We can therefore estimate the energy that a pulse must have for the wire to increase its temperature to 1000°C. Considering our situation, in the case of the wire of diameter of 200 μm, we have:

m =1 g, $\rho_{\rm CMN}$ = 8.90 g/cm^3, $c_{\rm p}$ = 0.41 J g^{-1} K^{-1}, $S = 2\ \pi$ r l = 6.28 cm^2, T = 1273 K, ΔT = 1000 K.

Hence, the three contributions become:

(A) $E = Q$ =410 J,
(B) P = 93.6 W $\rightarrow$ $E = P$ 0.07 s = 6.55 J,
(C) P = 6.28 W $\rightarrow$ $E = P$ 0.07 s = 0.44 J.

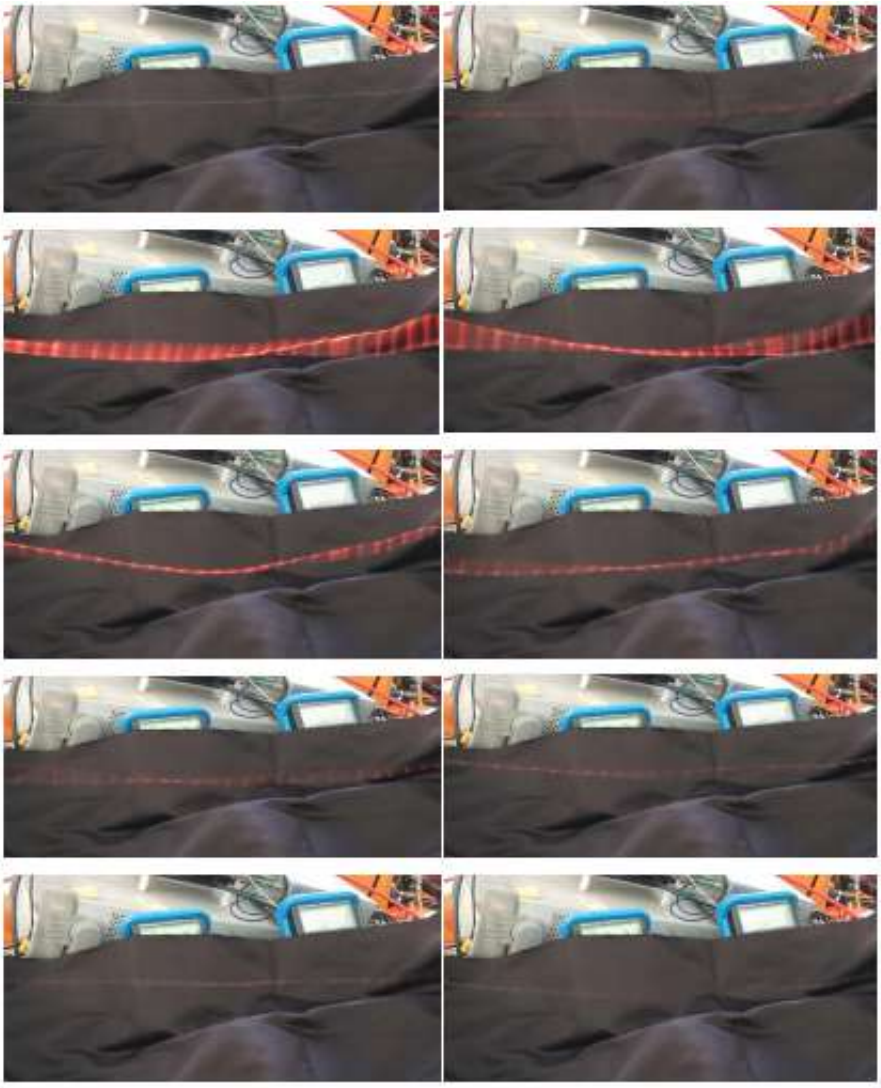

Figure 4. Photographic sequence of a 200-μm-diameter constantan wire subjected to High Peak Power Pulses: the time frame is about 20 ms and pulse duration is 70 ms. The brighter dots along the wire correspond to the knot sites, which reach higher temperatures than the other parts of the wire. In this way, local thermal non-equilibrium conditions are achieved.

The sum is $E = 417$ J, where the leading term is the one associated to the thermal capacity of the wire. The estimated mean pulse energy density is up to 800 J/g, an amount more than enough for our purposes.

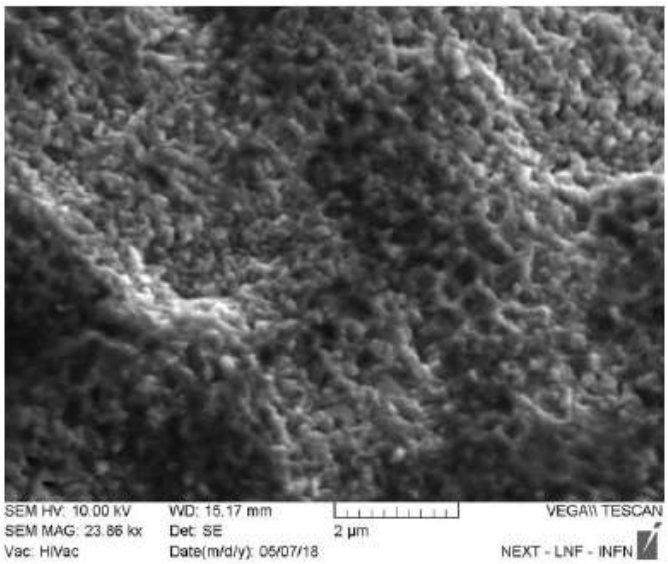

(**a**)

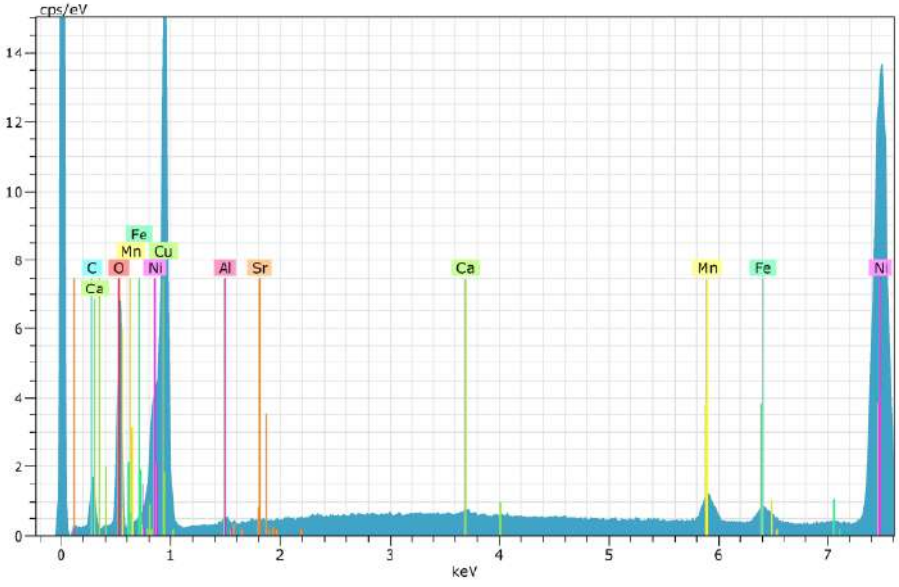

(**b**)

Figure 5. (a) SEM observation of the final part of the wire ($\Phi = 200\,\mu$m) taken as reference, just heated in air at 600°C for 300 s. (b) Corresponding EDX spectrum: counts per energy channel as a function of the incident X-ray energy. The highest count peaks correspond to Copper and Nickel.

Table 2. EDX spectrum analysis of the final part of the reference wire. Copper is present at 43.5% in weight, nickel at 31.6%.

Element	*Z*	Series	Count	C unnorm. (wt.%)	C norm. (wt.%)	C atom. (at.%)	C err. (1σ) (wt.%)
Cu	**29**	**K-series**	**167934**	**42.65**	**43.53**	**23.71**	**1.07**
Ni	**28**	**K-series**	**149 919**	**30.99**	**31.64**	**18.65**	**0.79**
O	8	K-series	22943	12.95	13.22	28.59	1.66
C	6	K-series	5231	9.39	9.58	27.61	1.48
Mn	25	K-series	7629	0.97	0.99	0.63	0.05
Fe	26	K-series	4387	0.56	0.57	0.35	0.04
Al	13	K-series	723	0.24	0.24	0.31	0.04
Ca	20	K-series	899	0.12	0.12	0.10	0.03
Sr	38	K-series	71	0.10	0.11	0.04	0.04

5. SEM Observations and EDX Analysis

We performed an analysis of the elemental content of the wire before and after the application of HPP procedure. For a different part of the wire we report SEM observation and EDX analysis. The maximum energy of electrons used in the spectroscopy is 30 keV, corresponding to a resolution of about 2 μm in depth. We have taken an untreated constantan wire, just heated at 600°C for 300 s in air, as reference for the comparison with a treated one. Figure 5 shows the SEM observation of the final part of such wire, while Table 2 reports the corresponding EDX analysis: the untreated wire is 43.5% Cu (by weight) and 31.6% of Ni.

After the wire is subjected to hundreds of HPP pulses, the external surface of the knot is treated with a water solution of mixed nitrates of Sr–Fe–K–Mn.

This treatment is executed by hand and repeated several times. Nitrates are subsequently decomposed to oxides by heating (up to 700–1000°C). Figure 6 and Table 3 show the composition on the surface of the knots. Here, Cu content is larger (58.40 wt.%) for the partial decomposition of CNM alloy – Cu has a lower melting temperature with respect to Ni – and the diffusion of the elemental Cu toward the surface. Note the increased amount of Fe (4.98 wt.%) and Sr (3.58 wt.%). Finally, the area between two knots, after the treatment, is shown in Fig. 7 and Table 4.

We can conclude that the relative composition of main materials (Cu, Ni) is *strongly* dependent on the position along the wire and varies largely according to the performed treatments and the geometrical position.

Table 3. EDX spectrum analysis of the area at the top of a knot after applying HPP procedure. Cu content has raised to 58.4 wt.%, due to its diffusion toward wire surface, while Ni is at 5.50%.

Element	Z	Series	Count	C unnorm. (wt.%)	C norm. (wt.%)	C atom. (at.%)	C err. (1σ) (wt.%)
Cu	**29**	**K-series**	**126 198**	**58.16**	**58.40**	**30.91**	**1.46**
O	8	K-series	11977	13.56	13.61	28.61	1.88
C	6	K-series	3187	10.58	10.62	29.74	1.83
Ni	**28**	**K-series**	**15 276**	**5.47**	**5.50**	**3.15**	**0.17**
Fe	26	K-series	19339	4.96	4.98	3.00	0.16
Sr	38	K-series	1359	3.57	3.58	1.38	0.16
Ca	20	K-series	4517	1.07	1.08	0.90	0.06
Mn	25	K-series	3598	0.88	0.89	0.54	0.05
Mg	12	K-series	552	0.70	0.70	0.97	0.08
Al	13	K-series	820	0.64	0.64	0.80	0.07

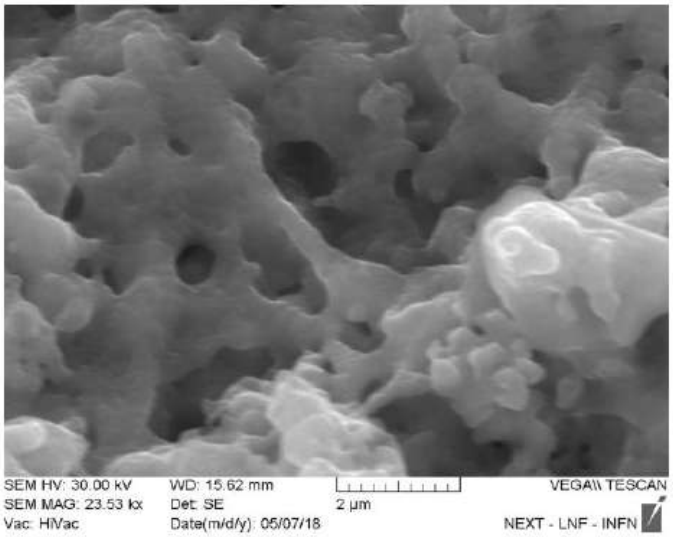

(**a**)

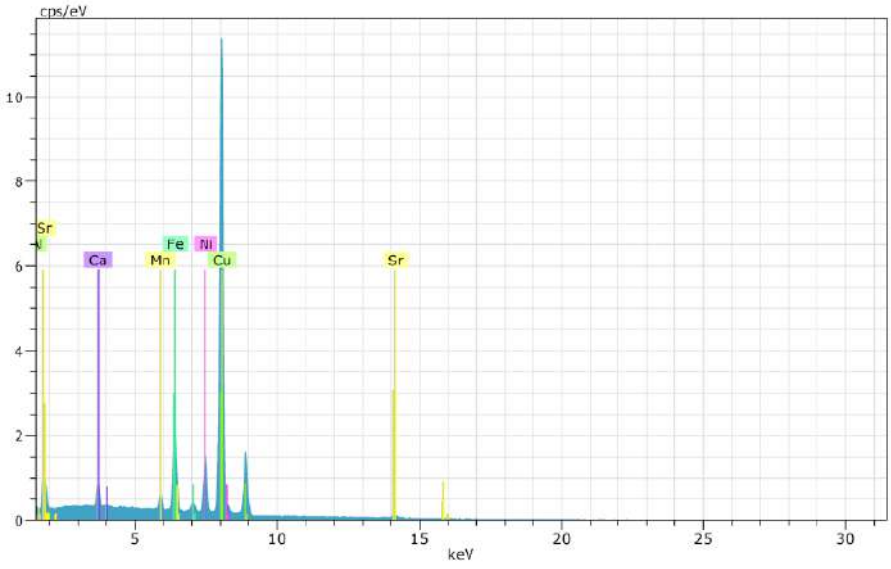

(**b**)

Figure 6. (a) SEM observation of a typical area at the top of the knots (wire with Φ =200 μm). (b) Corresponding EDX spectrum. Surface element composition changes remarkably after the application of HPP procedure, particularly as regards Nickel.

6. The Introduction of Fiberglass Sheaths

Since 2013, we have systematically adopted the procedure of putting the wires, immediately after their preparation, within a fiberglass sheath to prevent or minimize the separation of active surface layers from the wire core.

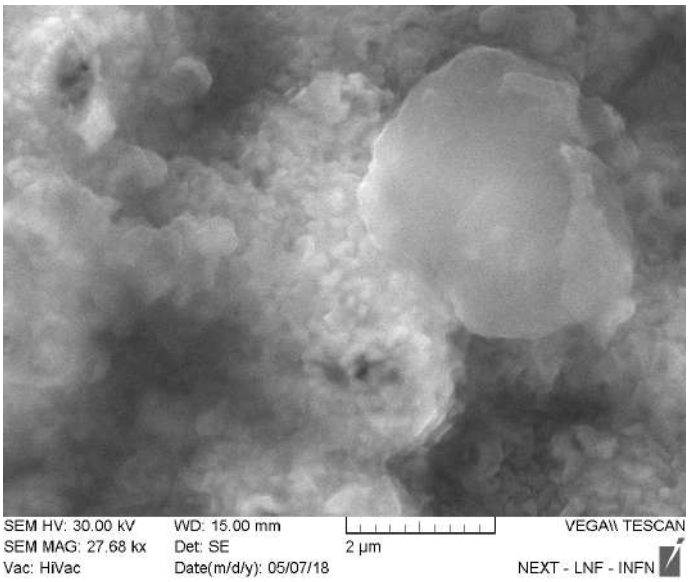

(**a**)

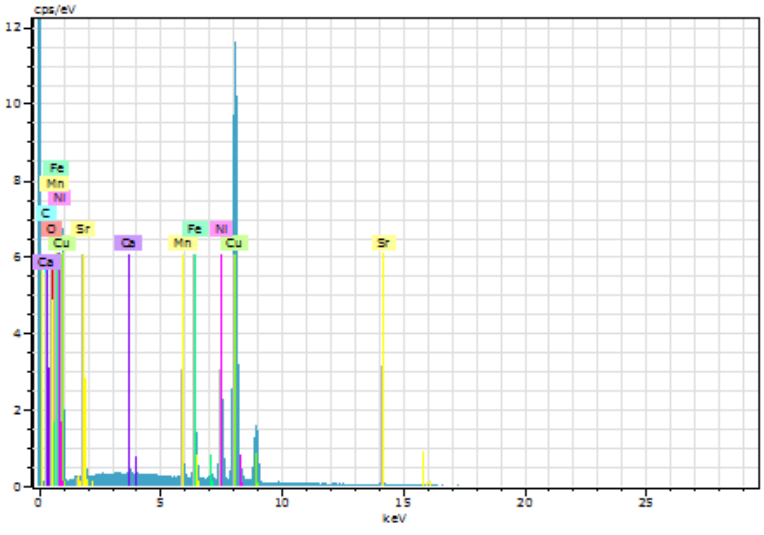

(**b**)

Figure 7. (a) SEM observation of the area between two adjacent knots (wire with Φ =200 μm). (b) Corresponding EDX spectrum.

We have reason to believe that this glass sheath may contribute to the generation of AHE under certain circumstances. We also observed this phenomenon in a previous set of experiments with palladium wires in 2008, where we employed them just for electrical insulation purposes. At that time, we tested several types of fiberglass sheaths and realized that Alumina (Al_2O_3)-based materials, although able to withstand quite large temperatures (T>1200°C), never produced significant excess heat effects. Only more common glass types such as E Glass, i.e. boro-silico-

Table 4. EDX spectrum analysis of the area between two adjacent knots. Cu is present at 62.5% in weight, Ni at 9.77%.

Element	Z	Series	Count	C unnorm. (wt.%)	C norm. (wt.%)	C atom. (at.%)	C err. (1σ) (wt.%)
Cu	**29**	**K-series**	**130 832**	**62.34**	**62.50**	**36.21**	**1.56**
O	8	K-series	11531	12.27	12.30	28.31	1.71
Ni	**28**	**K-series**	**26 135**	**9.75**	**9.77**	**6.13**	**0.27**
C	6	K-series	2364	8.17	8.19	25.11	1.51
Fe	26	K-series	13484	3.44	3.44	2.27	0.12
Sr	38	K-series	938	2.45	2.46	1.03	0.13
Mn	20	K-series	4477	1.11	1.11	0.74	0.06
Ca	25	K-series	928	0.22	0.22	0.20	

alumino-calcic glass, showed synergistic effects concerning AHE phenomena, although presenting limits on maximum continuous temperature of 550°C. In particular, we utilized the glass sheaths made by SIGI-Favier (IT-F), a derivative of borosilicate glass with further addition of TiO_2, Fe_2O_3 and Fe. We first thought that the glass itself could play an important role but we did not have any justification for our experimental observations yet.

Having in mind the idea of a "vessel" or containment made of micrometric fibers (diameter 4–6 μm, almost porous), we started modifying the sheaths by impregnation. This was done by dipping the sheaths into a solution of $Sr(NO_3)_2$ in H_2O or D_2O that was later decomposed to SrO at high temperature. Finally, we inserted the CNM wires into the impregnated sheaths.

We note that SrO has the feature of a low work function for electron emission, together with materials such as CaO and Y_2O_3. The use of these materials is in accordance with Yasuhiro Iwamura's procedures (1999) in the field of transmutations (Sr→Mo, Cs→Pr) induced by deuterium flux on multilayered (CaO, Pd) structures [9].

The work function W of a material is the main factor for electron emission at high temperatures. Such phenomenon is known as thermoelectric effect and is described by Richardson's law:

$$J = A_{\mathrm{g}} T^2 \exp\left(-\frac{W}{k_{\mathrm{B}} T}\right), \tag{2}$$

where J is the emission current density (A/m^2), $A_{\mathrm{g}} = \lambda_{\mathrm{R}}\, A_0$ is a constant factor (λ_{R} is a correction factor depending on the material, $A_0 = (q_{\mathrm{e}} m_{\mathrm{e}} k_{\mathrm{B}}^2)/(2\pi^2\hbar^3)$ =120.173 A cm^{-2} K^{-2}, with electron charge q_{e} =1.60$\times$ 10^{-19} C and electron mass m_{e} =5.11$\times$ 10^5 eV), T is temperature (in K), k_{B} = 8.617$\times$ 10^{-5} eV/K is the Boltzmann constant. At T constant, the reduction of only 1 eV of the work function implies an increase of the current density of a factor $\exp(1/(k_{\mathrm{B}}T))$. As an example, at T = 1000 K such factor is around 1.1$\times$ 10^5. In other words, a reduction from 2 to 1 eV increases the current density of a factor of 10^5! In Fig 8 Richardson's law is plotted for different values of the work function and one can clearly see how strongly dependent on it the current density is. Recent data show a value as low as 1.2 eV for SrO at low dimensionality with respect to 2.3 eV in bulk shape [10]. We produce thin layers of SrO at the surface of the glassy sheaths and mainly at CNM surface.

The atomic hydrogen produced by the dissociation of molecular hydrogen through the catalytic action of our sub-micrometric structured CNM wires is largely adsorbed onto the surface of the micrometric glass fibers. It is important to mention that the properties of some specific glasses with respect to their interaction with atomic hydrogen were discovered by Irving Langmuir around or before 1927. Langmuir selected the optimal type of glass for the construction of incandescent lamps, i.e. able to withstand repeated (>1000 times) fast cycling of temperatures (20→200→20°C) without self-damaging. We believe that the impregnation steps with SrO, Fe_xO_y and K–Mn, as a whole, further enhance the intrinsic tendency of borosilicate glass fibers to absorb or interact with atomic hydrogen. Moreover,

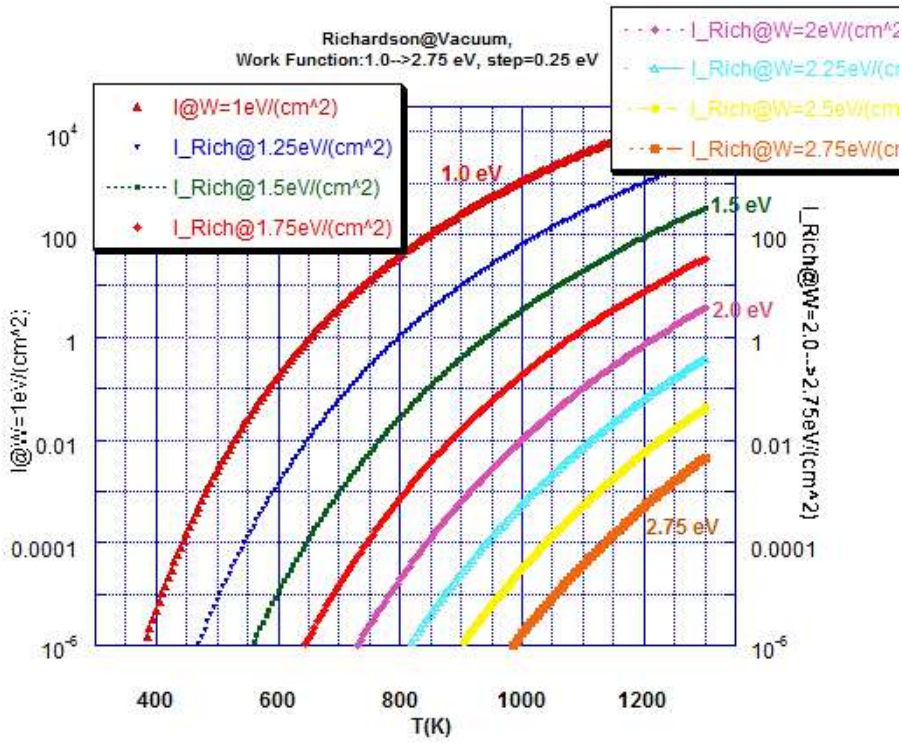

Figure 8. Plot of Richardson's law: current density versus temperature for values of work function ranging from 1 to 2.75 eV with a step of 0.25 eV. The scale is semilogarithmic.

the "chemically aggressive" alkaline elements used for impregnation and drying by high temperatures increase the surface area of glassy sheaths. The atoms being much closer to each other compared to atoms in free motion in a gas, the formation of a thin film of atomic hydrogen adhering to glass surface increases the probability of hydrogen recombination in its molecular form, an exothermic reaction with the release of 4.52 eV. We think that glass adsorption is therefore a cofactor in the generation of excess heat together with the main LENR process and we cannot exclude the possibility that the H film act as a reservoir for the diffusion process of atomic hydrogen into the metallic wires [11].

We presented the main results of our experiments at "2014 MIT Colloquium on Cold Fusion effect" (21–23 March 2014;IT Cambridge, USA). The reactor consisted of two constantan wires and one Pt wire, inserted inside glass sheaths, braided around the central stainless steel (SS) support and, finally, this latter covered with a fiberglass sleeve. The whole reactor is inserted and thermally sealed in a thick borosilicate glass tube. In order to definitively clarify the role of the glass in heat generation, we repeated the experiment with two additional sleeves on the steel support and compared the results. Temperature data in Fig. 9 clearly show the positive role of glass in heat generation and present behavior growing at low pressure, in accordance with Langmuir's observations about hydrogen recombination. Hydrogen recombination reaction is highly exotermic: in principle, the local temperature can be as high as 36 000 K at very low pressures.

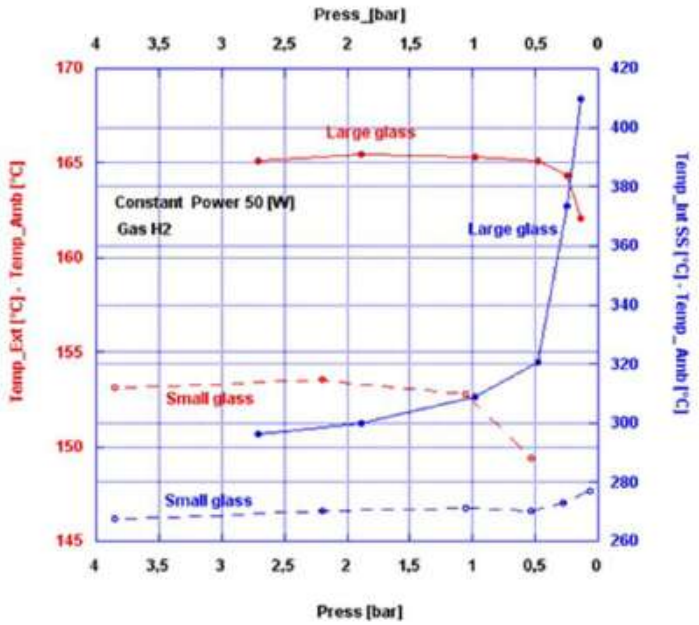

Figure 9. Data comparison for tests conducted with a small and a large amount of glass enveloping the SS support in the reactor, in H_2 atmosphere and at constant input power of 50 W. Temperature difference with ambient at the external glass tube surface (*red*) and at the central SS tube (*blue*) is plotted against pressure in the reactor.

7. The Introduction of Iron and Potassium

After consuming the first batch of constantan wires (excess heat up to 5–20% of the input power at 50 W input), the use of new batches resulted in a lower AHE, although using the same reactor operated in the isoperibolic regime. We later realized that the first batch of CNM that we used was prepared before 1970. We measured that the Fe content, either as an impurity or intentionally added, was as large as 0.5–1% on average, while in certain spots it could reach 3–5% concentration, especially at the surface. In addition to the lower purity of starting materials (i.e. Cu, Ni, and Mn), we have considered possible contamination of the surface during the swaging process and/or inappropriate storage in a rusted iron cupboard. Moreover, if we consider that the aforementioned J-type thermocouples also contain iron, the case for its synergistic effect on AHE is strongly reinforced.

It is worth mentioning also that iron has the unusual property of absorbing H_2 at high temperatures ($T > 600°C$) and releasing it at lower temperatures. Aiming to further increase AHE, we eventually decided to add Fe together with K, as mixed oxides, on the surface of the wires and sheaths as a dissociation promoter of $H_2 \rightarrow 2H$ reaction. We were inspired by Fischer–Tropsch and Bosch–Haber type catalysts for the synthesis of gasoline and ammonia. The role of K was brought to our attention by C. Lorenzetti (co-author) in 2014. The addition of iron was made before treating the wires with the HPP procedure. Later, in May 2016, we added also Mn in order to stabilize the observed effects, thanks to Mn ability of reducing the evaporation of K at high temperatures [12,13]. Just as a similarity, the effect of Mn resembles that of Iodine to extend the useful life span of the well-known incandescent (halogen tungsten) lamps.

Table 5. Effect of argon, xenon and heavy water (D_2O) addition on temperatures measured in the reactor for Cst71 wire at 50 W input power.

Gas type	D_2	Xe / D_2	Xe / D_2	Ar / D_2	He	H_2	D_2O (2 cm^3) Air (10 cm^3)	D_2O (2 cm^3) Air (10 cm^3) Xe (45 cm^3)
P at reactor off (bar)	1	1 / 0.8	1 / 0.8	1 / 1	1	1		
P at reactor on (bar)	1.41	2.63	2.64	2.71	1.346	1.32	0.20	0.51
P_w (W)	50.18	50.13	50.38	49.91	49.75	50.25	50.11	50.30
T_c (°C)	197.2	208.3	208.6	205.5	191.03	192.8	203.73	212.42
T_{ss} (°C)	258	342	342.9	308.9	253.5	243.7	367.8	400.08
T_{Pt} (°C)	257	318	319.4	292.26	252.1	244.6	344.69	376.14
T_{amb} (°C)	20.7	20.4	19.98	18.35	17.04	17.8	20.53	20.57

8. Introduction of Noble Gases with Low Thermal Conductivity

Since 2008, we have observed that the addition of argon and other low-conductivity noble gases to H_2 or D_2 increases the likelihood of AHE occurrence. This was noticed even in experiments conducted at low pressure, e.g. at 0.1 bar.

Our motivation for inert gas addition was to reduce the applied input electric power thanks to lower thermal conductivity losses, allowing, for instance, the enhancement of the detection of very small AHE. Such effect was further magnified when Ar was replaced with Xe, the gas with the lowest value of thermal conductivity among the non-radioactive, $\kappa = 5.5$ $mWm^{-1}K^{-1}$ at 300 K and 1 bar.

For xenon in particular, we were able to measure an AHE magnitude much larger than expected.

At the end of November 2016, while still trying to interpret the effect of xenon on AHE, we found with great surprise a 1993 German patent (DE4300016) claiming the addition of xenon to deuterium to enhance the reaction $2D^+ \rightarrow He^4$ [14]. We also noticed similarities in the experimental apparatus where this reaction is supposed to occur, a thin glass tube containing ionized Xe and D.

In Table 5 we compare temperature values of measurements performed at 50 W input power on Cst71 wire ($\Phi = 200$ μm) for various combinations of gas mixtures. It is noticeable the rise in temperature when noble gases are added to reactor atmosphere, a phenomenon more pronounced in the case of Xe, showing that such gases play a role in the generation of AHE, may be acting as catalyzers.

9. Air Flow Calorimetry

In our experiments, we have always used isoperibolic calorimetry to measure the heat generated by the reactor and exchanged with the ambient air. Thermometers are placed in proper sites of the reactor, such as at the SS central tube and at the external wall of the borosilicate glass tube, and temperatures constantly monitored. In this way, we are able to estimate the heat radiated by the reactor wall (Stefan–Boltzmann law) and the heat lost by convection to ambient (Newton's law of cooling). The sum of these contributions gives the calculated heat produced by the reactor. Isoperibolic calorimetry has revealed to fit very adequately the requirements for LENR experiments, as it allows working in non-equilibrium conditions, fundamental to get and maximize AHE. We measured gains near a factor 2 in the experiments at the highest temperature, although with limited stability over time.

Over the years, the scientific debate produced evidence that local measures taken at specific spots may lead to an overestimate of the actual total amount of heat, and therefore of energy, outgoing from the reactor. Mass-flow calorimetry is considered a more reliable type of measurement, as the heat produced is exchanged with a substance flowing in a controlled environment where temperature tends to be homogeneous. When applied to our experiments,

Table 6. Values of density, specific heat and maximum water content of air (temperature range 0–100°C, 1 atm).

T (°C)	Density (kg/m^3)	C_p (kJ/kg K)	Max H_2O content (g H_20/m^3 air)
0	1.292	1.005	4.84
5	1.268	1.005	6.78
10	1.246	1.005	9.37
15	1.225	1.006	12.77
20	1.204	1.006	17.19
25	1.184	1.006	22.88
30	1.164	1.006	30.1
35	1.146	1.006	39.2
40	1.127	1.007	50.60
45	1.11	1.007	64.63
50	1.093	1.007	81.85
55	1.076	1.007	102.82
60	1.060	1.008	128.1
70	1.029	1.009	194.6
80	1.000	1.009	194.6
90	0.973	1.010	414.7
100	0.946	1.011	584.5

however, the reactor does not operate under the optimal conditions for obtaining AHE and performances are expected to be lower.

In the light of such considerations, we have decided to replicate the experiments in air-flow calorimetry, aiming to prove in a more rigorous way the excess power generated by the active reactor.

The air flow calorimeter operates according to the simple formula:

$$Q = mc_\mathrm{p}\Delta T, \tag{3}$$

where Q is the heat exchanged, m air mass (kg), c_p the specific heat (kJ/kg K), ΔT is the temperature difference between outcoming and incoming air (K). Difficulties arise because, being a gas, air density decreases a great deal with increasing temperature, while c_p increases only slightly. Moreover, air water content increases a great deal with temperature. The energy needed inside the measuring chamber to increase water temperature (4.184 J/g) or even evaporate it (i.e., phase transition) can be large. Such water is a negative term in the system. Table 6 shows air density, specific heat and maximum water content for temperature ranging from 0 to 100°C, used in our calculations. We made a consistent effort during the measurements to keep room temperature constant and room humidity in the chosen range. We controlled such quantities by means of an air-conditioner working also in dehumidification mode and verified with an hygrometer that relative humidity was maintened between 45 and 55%.

The calorimeter consists of a large insulating Styrofoam box whose internal walls are covered with a layer of thick aluminum foil in order to make the temperature uniform. During the experiments, the external wall of the glass reactor is covered with a double layer of black and thick aluminum foil to further homogenize the internal temperature. For calibrations, we have used a halogen tungsten lamp, with maximal power 230 W, but underpowered during operations in order to reduce temperature. We have put the lamp inside a borosilicate glass tube with the same composition and dimension as that of the reactor ($L = 29$ cm, $\Phi = 34$–40 mm), as shown in Fig. 10. Calibrations have been performed powering the lamp in a whole cycle 0 $\rightarrow$120 W $\rightarrow$ 0, with steps of 20 W.

Figure 11 summarizes the results of the experiments conducted in air-flow calorimetry. The variation of temperature ΔT between outcoming and incoming air, divided by input power (°C/W), is plotted against the given input

Figure 10. Interior of the air-flux calorimeter with the reactor (*above*) and the Halogen Tungsten lamp used for calibration (*below*, max power 230 W). The lamp is inserted inside a borosilicate glass tube of the same dimensions of that used for the reactor. The internal walls of the insulating box are covered with an aluminum foil in order to make temperature as uniform as possible inside the calorimeter.

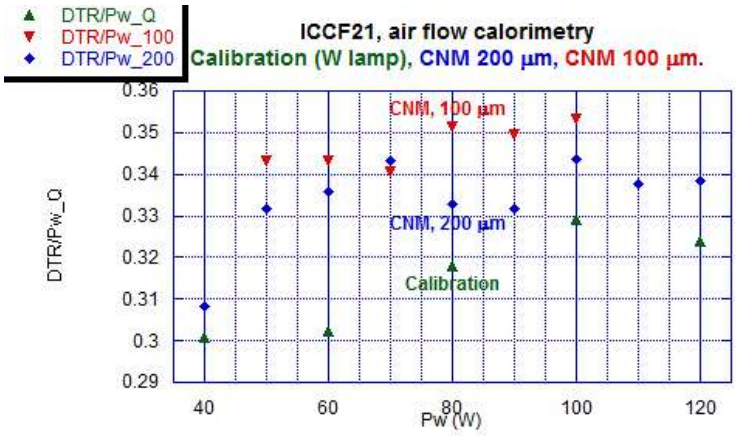

Figure 11. Comparison of the results obtained with experiments conducted with air-flow calorimetry. The change in temperature between outgoing and incoming air divided by the input power ($\Delta T/P$), is plotted against the input power (P). The first series of measurements (*in green*) are performed giving power to the calibration heater, a halogen tungsten lamp. Red points correspond to the measurements taken with the reactor operating with 100-μm diameter CNM wire, and they are interrupted at 100 W because of the breaking of the wire. In blue, the points referring to the reactor with 200-μm diameter CNM wire. The wires are in an atmosphere of deuterium D_2 at 1.2 bar at room temperature. Data above the calibration curve indicate the production of AHE.

Figure 12. Picture of the borosilicate glass reactor after last experiment with air-flow calorimetry: it is clearly visible, at center, the imprint of the sheaths caused by partial melting of the internal wall due to local overheating.

power (W). The green points define the calibration curve obtained with the tungsten lamp. The red points correspond to measurements using a CNM wire of 0.1 mm of diameter, which broke after only 840 s at 100 W of input power. Finally, the blue points show the measurement with a CNM wire of 0.2 mm diameter. The reactor operated in a D_2 atmosphere, with pressure of 1.2 bar at room temperature. All the data shown are raw; i.e. without corrections for air density inside the thermal-insulating calorimeter box. Only external room temperature and humidity are kept almost constant. Moreover, with increasing temperature the heat losses increase by external air convection from the large insulating box to ambient. We made some cross checks of the results from time to time, by calculations using the value of Table 6 and by measuring the temperature of the external wall of the insulating box through a high sensitivity (0.1°C) IR video-camera (Nikon). We can clearly observe that the points corresponding to the active reactor are above the threshold given by the calibration curve, indicating therefore the production of excess heat. We note that the data are very conservative, as we were very careful not to overestimate any contribution.

The best results obtained are the following:

(a) With a CNM wire with diameter 100 μm, D_2 atmosphere at 1 bar, internal reactor temperature 500°C, input power 90 W, the AHE was over 12$\pm$2 W, i.e. over 150 W/g, but after 1 day the wire broke. In details, when supplied with 100 W, the wire broke only after 840 s; we estimated from the behavior an excess power of about 30 W, but, of course, it is just a guess because of the lack of satisfactory data points.
(b) With a CNM wire with a diameter 200 μm, it was necessary to use a Xe–D_2 mixture (each 0.1 bar) and input power of 120 W in order to obtain an AHE of 6–7 W stably for weeks.

As proof of the high temperatures reached by the wire, after the reactor was switched off and opened, we observed

that some overheated segments of the fiberglass sheaths partially melted the internal wall of the borosilicate glass tube and left their imprint on it (Fig. 12). According to the specifics of the Schott Duran glass used, the softening temperature is 825°C.

10. Addendum in Response to Private Questions Received during and after the Presentation: toward a New Reactor Design and Similarities with a Thermionic Diode

In 2014, a second independent constantan wire was introduced in the reactor. When the first treated wire was heated passing a current into it, we observed a weak current flowing in the second wire as well as the rise of a voltage with respect to the first. Moreover, the phenomenon is clearly driven by a temperature difference of several hundred degrees Celsius between the cathode (heated via direct current) and the anode. (It is important to note that the wires comprise a surface with a low work function due to the presence of oxides of alkaline metals, typically between 1 and 2.5 eV, depending on surface morphology.) The spontaneous current and voltage were also observed independently by Mathieu Valat and Bob Greenyer using a measurement set-up arranged by them completely independently of our work

This voltage turned out to be the consequence of the thermionic emission from the first wire that behaved as a cathode while the second wire as an anode. Given the relatively high pressure at which the phenomenon was observed, the exchange of charge between the first wire (cathode) and the second wire (anode) is supposed to be mediated by ions. After much work to stabilize the phenomenon, we recognized that the current density produced in the non-connected wire, according to preliminary data analyses, is quite well described by Child–Langmuir law

$$J = K \frac{V^{3/2}}{d^2}\,, \tag{4}$$

where the current density J is proportional to the three-halves power of the differential of potential between cathode and anode and inversely proportional to the square of their distance. Consequently, the amount of spontaneous current was dependent on the sign of the current, i.e. the potential, applied to the cathode wire.

Interestingly, the voltage arising between the two wires did show a strong correlation with AHE. In a set of still on-going experiments, an external voltage (bias) was applied between the cathode (the treated wire heated by direct current) and the anode through an external power supply, leading to an AHE increase sufficient to melt the cathode. These observations draw attention to the stunning similarities between the reactor and a thermionic diode. Furthermore, we can elaborate on the possibility of converting the AHE generated on the cathode into electricity using its thermionic emission. In other words, the on-going work is exploring a highpressure thermionic converter where the cathode is heated by an AHE occurring on it, or in close proximity [15]. In this reactor configuration, AHE will be driven by the voltage between the two electrodes and by their temperature. While part of the electrical output of this converter will be used to control the reactor (i.e. maintaining a certain temperature of the cathode), the remaining part could be used for an external load.

11. Conclusion

With this last set of experiments, we have observed that the whole of procedures adopted, such as:

- The use of constantan – our main original contribution in LENR research – as a catalytic material for molecular hydrogen dissociation, able to reduce its resistance in correspondence with atomic hydrogen/deuterium absorption [16].
- The pulsed oxidation of constantan wires through the High Peak Power procedure, to increase surface area and form layered nanostructures on wire surface [16].

- The addition of potassium modified iron oxides as a hydrogen dissociation catalyst [11].
- The use of fiberglass sheaths impregnated with solutions of strontium nitrate – an electron emitter – and iron nitrate/potassium permanganate in D_2O [11,17] (decomposed to oxides).
- The use of manganese to stabilize the system over time, reducing potassium evaporation [11,17].
- The introduction of knots with small-diameter holes along the wire, to enhance non-equilibrium conditions, being the knots location of thermal and magnetic gradients [11].

allows the production of AHE – although at levels quite lower than with isoperibolic geometry – even when using flow-calorimetry measurement techniques, which typically *minimize* the non-equilibrium situations. Wire temperature appears to be a key factor and has to be as high as possible, while avoiding the sintering of sub-micrometric materials.

The amount of AHE is inversely proportional to the wire diameter, because, for a given power, a thinner wire reaches higher temperatures. On two occasions we have observed that the 100-μm diameter constantan wire is *not* able to sustain, for a long enough time, an input power close to 100 W in our experimental conditions (length about 130 cm, 115 cm after tying the knots). In this regime, the AHE values grow too fast, perhaps in a positive feedback process.

We also have indications that the voltage drop along the wire (i.e. NEMCA effect [8]) plays an important role in AHE generation. Further systematic work is needed to keep under full control such extremely interesting results and operating regimes.

From the point of view of futuristic technological applications, we note that the maximum excess power density, with 100-μm diameter wire, was larger than 100 W/g, supposing that also the bulk of the wire, not only surface, is operative. On the other hand, if we suppose that the glassy sheaths, wetted with the usual mixture of Sr–Fe–K–Mn (total weight of about 3 g), played a special role for AHE generation, the power density drops largely. Anyway, the industrial cost of glassy sheath is quite low, a few Euros per gram.

Such values are qualitatively similar to our previous experiments (up to 2008), when we used mainly long Pd wires (diameter of 50 and 100 μm) treated with several cycles of deposition of specific materials (Th-nitrate, Sr-nitrate, liquid glass home-made) and inserted in glassy sheaths. Sadly, almost all relevant logbooks, where all the details and know-how were reported, were scrapped by people working at LNF in February 2015.

For the last 10 days before the ICCF21, a new reactor has been operating, with minor changes in the overall geometry. Our aim is to reconfirm the previous data and increase, step by step, with the input power controlled to avoid uncontrolled self-breaking/burning of the wire. The first results at low power are similar to the previous experiment just reported. With regard to the measurement devices, the realization of an air-flow calorimeter with higher accuracy is an on-going activity parallel to the development of the reactor.

Acknowledgments

The experimental work described in this paper was carried out mainly at INFN-LNF; some key trials were conducted at the premises of a LENR Laboratory located in a Metallurgical Company of North Eastern-Italy, which has also helped financially since 2011. Società Italiana di Guaine Isolanti (SIGI) designed and produced innovative/unconventional types of glassy sheaths among a joint collaboration with our Group, the Favier Company (France side of SIGI) and the aforementioned Metallurgical Company. The replication of previously selected experiments was also attempted within Martin Fleischmann Memorial Project by Mathieu Valat and Bob Greeyner with the Live Open Science approach. We are indebted to Prof. Brian Josephson, Nobel Laureate in Physics (who has long been involved in the LENR field) for his "Open Letter" addressed also to the Scientific Coordinators of INFN, where he asked for the continuation of F. Celani's LENR Research in Frascati even after the retirement age limit. We heartily thank Laura Vantini for her promotion of a petition on the website platform Change.org asking for the conservation of our laboratory at INFN-LNF and its availability to F. Celani after his retirement. The petition was addressed to the President of the Italian

Republic to the Prime Minister of the Government and to the Minister of Education, Universities and Research and it was presented to them on 21 October 2017 [18]. In September 2017, F. Celani was thoroughly interviewed by Pandora TV, a Web TV whose responsible Giulietto Chiesa, a former member of European Parliament, is very interested in energetic and environmental problems [19]. An interview with F. Celani by the journalist Alessandro Milan was published on the newspaper "La Verità" in September 2017, in agreement with the deputy editor Massimo De Manzoni [20]. Both people are very involved, in their professional activity, in issues concerning sustainable development and low environmental impact technologies Starting from October 2017, an important political Group in Italy (North League) pushed the President of INFN to allow the continuation of F. Celani's experiments in the Frascati Laboratory, although he had reached the age-limit of retirement. The main people involved were Francesco Malagoli, Filippo Panini, Paolo Varini (from Modena City). All of them have followed LENR studies since 2010, among their key political framework/projects on environmental conservation and pollution reduction.

Antonino Cataldo and Stefano Bellucci (NEXT collaboration) performed SEM and EDX analysis at INFN-LNF. Expenses at ICCF21 were partially supported by IFA organization (main topics are "Water and Energy"-Italy. We are indebted to both Jed Rotwell (USA) and Jean Paul Biberian for their invaluable work to improve the paper about our (several) misprintings and Italian–English neologisms.

References

[1] F. Paneth and K. Peters, Über die Verwandlung von Wasserstoff in Helium, *Naturwissenschaften* **14** (43) (1926) 956–962.
[2] M. Fleischmann, S. Pons and M. Hawkins, Electrochemically induced nuclear fusion of deuterium, *J. Electroanal. Chem.* **261** (1989) 301.
[3] S. E. Jones, E. P. Palmer, J. B. Czirr, D. L. Decker, G. L. Jensen, J. M. Thorne, S. F. Taylor and J. Rafelski, Observation of cold nuclear fusion in condensed matter, *Nature* **338** (1989) 737–740.
[4] A. De Ninno, A. Frattolillo, G. Lollobattista, L. Martinis, M. Martone, L. Mori, S. Padda and F. Scaramuzzi, Emission of neutrons as a consequence of titanium–deuterium, *Il Nuovo Cimento* A **101** (5) (1989) 841–844.
[5] S. Focardi, R. Habel and F. Piantelli, (Anomalous Heat Production in Ni-H Systems,(*Il Nuovo Cimento A,* vol. 107, pp. 163-167, 1994.
[6] S. Romanowski, W. M. Bartczak and R. Wesołkowski, Density functional calculations of the hydrogen adsorption on transition metals and their alloys. An application to catalysis, *Langmuir* **15** (18) (1999) 5773–5780.
[7] B.S. Ahern, K.H. Johnson and H.R. Clark Jr., Method of maximizing anharmonic oscillations in deuterated alloys, Patent US5770036, US5411654, US5674632, 23 June 1998.
[8] C.G. Vayenas, S. Bebelis and S. Neophytides, Non-Faradaic electrochemical modification of catalytic activity, *J. Phys. Chem.* **92** (1988) 5083–5085.
[9] Y. Iwamura, T. Itoh and M. Sakano, Nuclear products and their time dependence induced by continuous diffusion of deuterium through multi-layer palladium containing low work function, *Proc. of ICCF8,* 2000, pp. 141–146.
[10] T.J. Sommerer, Barium-free electrode materials for electric lamps and methods of manufacture thereof, Patent WO2007064570 A2, 7 June 2007.
[11] F. Celani, A. Spallone, B. Ortenzi, S. Pella, E. Purchi, F. Santandrea, S. Fiorilla, A. Nuvoli, M. Nakamura, P. Cirilli, P. Boccanera and L. Notargiacomo, Observation of macroscopic current and thermal anomalies, at high temperatures, by hetero-structures in thin and long constantan wires under H_2 gas, *J. Condensed Matter Nucl. Sci.* **19** (2016) 29–45.
[12] A. Miyakoshi, A. Ueno and M. Ichikawa, Mn-substituted Fe–K mixed oxide catalysts for dehydrogenation of ethylbenzene towards styrene, *Appl. Catalysis* A*: General* **216** (2001) 137–146.
[13] A. Kotarba, I. Kruk and Z. Sojka, How the iron oxide catalyst for EBDH is stabilized via Mn addition, *J. Catalysis* **221** (2004) 650–652.
[14] H. Preusker, Design of a helium fusion reactor, Patent DE4300016, 02 01 1993.
[15] K.A.A. Khalid, T.J. Leong and K. Mohamed, Review on thermionic energy converters, *IEEE Trans. Electron Devices* **63** (2016) 2231–2239.

[16] F. Celani et al., Experimental results on sub-micro structured Cu–Ni alloys under high temperatures hydrogen/deuterium interactions, *Chem. Mater. Res.* **3**(3) (2013) 25–76.
[17] F. Celani, G. Vassallo, E. Purchi, S. Fiorilla, L. Notargiacomo, C. Lorenzetti, A. Calaon, B. Ortenzi, A. Spallone, M. Nakamura, A. Nuvoli, P. Cirilli, P. Boccanera and S. Pella, Improved stability and performance of surface-modified Constantan wires, by chemical additions and unconventional geometrical structures, *J. Condensed Matter Nucl. Sci.* . **27** (2018) 1–13.
[18] L. Vantini, No alla distruzione del laboratorio di Francesco Celani, 21 Oct 2017 Online. Available: https://www.change.org/p/sergio-mattarella-no-alla-distruzione-del-laboratorio-di-francesco-celani.
[19] Pandora TV, Francesco Celani: Una scienza, dogmatica impedisce la ricerca e danneggia il paese , (27 Sept. 2017. Online. Available: https://www.pandoratv.it/francesco-celani-una-scienza-dogmatica-impedisce-la-ricerca-e-danneggia-il-paese/.
[20] A. Milan, Uno scienziato contro il Monopolio, 23 Sept. 2017. Online, Available: http://edicola.laverita.info/laverita/books/laverita/2017/20170923laverita/#/1/.